Proceedings of the 9th U.S. National and 10th Canadian Conference on Earthquake Engineering
Compte Rendu de la 9ième Conférence Nationale Américaine et
10ième Conférence Canadienne de Génie Parasismique
July 25-29, 2010, Toronto, Ontario, Canada • Paper No 1465

EXPERIMENTAL AND ANALYTICAL ASSESSMENT OF SHEAR-CONTROLLED WALL RESPONSES

L. Massone[1], K. Orakcal[2] and J. W. Wallace[3]

ABSTRACT

In the mid-1900s, use of lightly reinforced, perimeter walls with openings was fairly common. A large number of hospital buildings in California, constructed between 1950 and 1970, included lightly reinforced wall piers (vertical wall segments) and wall spandrels (horizontal wall segments). Therefore, accurate assessment of the as-built strength, stiffness, and deformation characteristics of lightly reinforced wall piers and spandrels could have a substantial impact on the evaluation and rehabilitation process, as well as the cost associated with the rehabilitation. Accordingly, an experimental program was conducted at UCLA on selected lightly reinforced wall pier and spandrel configurations to investigate various response attributes including shear strength, stiffness, and deformation capacity, as well as the effect of outdated construction practices such as using one curtain (vs. two) of distributed web reinforcement, discontinuity of reinforcement at a possible weakened plane joint, and the lack of hooks on transverse reinforcement, on the shear strength and lateral load behavior. Test results were compared with ACI shear strength equations and FEMA 356 lateral load vs. deformation backbone relationships to assess the reliability of these documents or the conservatism embedded therein, pertaining to seismic evaluation and rehabilitation of existing buildings. Furthermore, a comprehensive modeling approach, which incorporates flexure-shear interaction, was implemented, validated, and improved upon using test results.

Introduction

The experimental program conducted at the UCLA Structural/Earthquake Engineering Research Laboratory involved testing of six wall pier (WP) and eight wall spandrel (WS) specimens, with dimensions, reinforcement configuration, and material properties based on as-built conditions for two hospital buildings constructed in California in the early 1960's utilizing perimeter walls for lateral load resistance. The specimens were 3/4-scale, and comprised specific construction features commonly used in construction at that time, including use of a single curtain of distributed reinforcement, lack of hooks on transverse (web) reinforcing bars, and existence of

[1]Assistant Professor, Dept. of Civil Engineering, University of Chile, Blanco Encalada 2002, Santiago, Chile
[2]Assistant Professor, Dept. of Civil Engineering, Bogazici University, 34342 Bebek, Istanbul, Turkey
[3]Professor, Dept. of Civil & Env. Engineering, University of California Los Angeles, Los Angeles, CA 90095

weakened plane joints (where the concrete cross-section is reduced and part of the longitudinal reinforcement is discontinued in order to initiate cracking). A detailed description of the complete experimental program can be found elsewhere (Massone, 2006; Orakcal *et al*., 2009).

Specimen Description, Test Setup, and Observed Failure Modes

The spandrel specimens were 152 cm tall, 152 cm long, and 15 cm thick, whereas the piers were 122 cm tall, 137 cm wide, and 15 cm thick. Details of the specimens are presented in Table 1. Four different types of wall spandrel (WS) specimens were tested, with two identical specimens of each type. Type 1 (Fig. 1a) and 2 specimens were differentiated primarily by the amount of the longitudinal reinforcement provided at wall boundaries, whereas for Type 3 and 4 specimens, 180-degree hooks were not provided on the transverse reinforcement and a lower longitudinal web reinforcement ratio was used. In addition, the location of the weakened plane joint (WPJ) for Type 3 and 4 specimens was varied. The WPJs considered also cutting a portion of the longitudinal web bars at the location of the WPJ. The WPJ was located at wall mid-height for specimen Types 1, 2, and 3, whereas it was located at a distance of 25 mm [1 in.] from the bottom wall-pedestal interface for Type 4 specimens. Longitudinal reinforcing bars provided at wall boundaries ("jammed" bars) were continuous over the height of the specimens. All six of the wall pier (WP) specimens were identical in geometry and reinforcement detail (Type 5 - Fig. 1b). The pier specimens were subjected to axial load levels of 0%, 5% and 10% of their axial load capacity ($A_g f'_c$). There was no WPJ on the piers; the longitudinal web bars and the boundary bars were continuous over the height of the specimen. No hooks were provided on the transverse reinforcement.
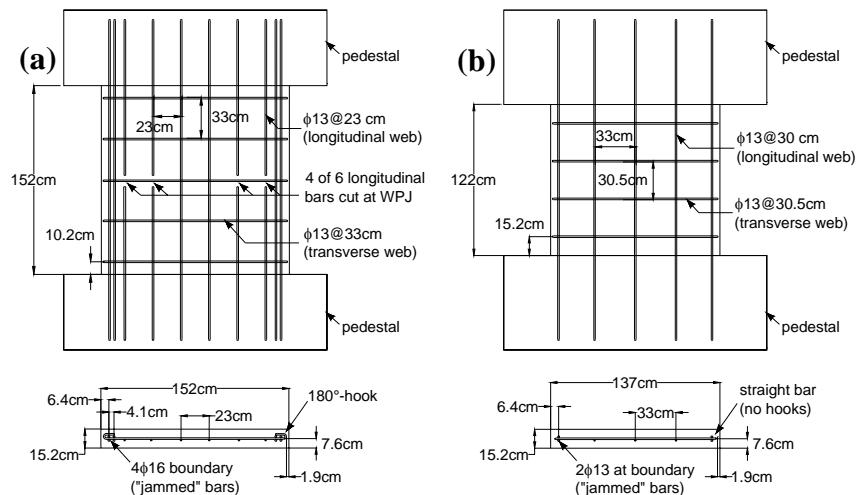

Figure 1.   Wall specimen geometry and reinforcement.
(a) Wall spandrel (type 1), (b) Wall pier (type 5).

Relatively low shear-span-to-depth ratios were achieved during testing of the specimens via fixing the base of the walls, restraining rotations at the top of the walls, and applying the lateral load at specimen mid-height. Reversed cyclic lateral loads were applied at the mid-height level of the specimens, through a horizontal actuator connected to the loading frame. An extensive set of instrumentation was provided during the test program for measuring loads, displacements, average deformations, and strains at various locations on the wall specimens. LVDTs were mounted diagonally (in an "X" configuration), vertically, and horizontally and at specified locations on the specimens to measure the magnitude and distribution of shear deformations, flexural deformations, sliding shear deformations, and average normal strains in longitudinal and transverse directions, among others. The instrumentation used during the test program is described in detail by Massone (2006) and Massone *et al*. (2009).

Table 1.   Properties of and test results for wall spandrel (WS) and wall pier (WP) specimens

| Specimen | | Test | t_w | l_w | h_w | $M/(Vl_w)^{(1)}$ | Transv. Reinf. | | Long. Reinf. | | Boundary | Axial Load | VTEST | VTEST |
ID No.	Type	No.	(cm)	(cm)	(cm)		ρ_t (%)	Hooks	ρ_l (%)	Cut Bars	A_{sb} (cm²)	$N/A_g f'_c$ (%)	Vn,FEMA[4]	Vn,ACI-SF[5]
WS-T1-S1	1	test1	15.2	152	152	0.50	0.278	Yes	0.428	4 of 6[3]	8	0	1.44	-
WS-T1-S2		test4	15.2	152	152	0.50	0.278	Yes	0.428	4 of 6[3]	8	0	1.41	-
WS-T2-S1	2	test2	15.2	152	152	0.50	0.278	Yes	0.400	4 of 6[3]	3.29	0	0.96	-
WS-T2-S2		test3	15.2	152	152	0.50	0.278	Yes	0.400	4 of 6[3]	3.29	0	1.04	-
WS-T3-S1	3	test11	15.2	152	152	0.50	0.278	No	0.256	2 of 4[3]	2.58	0	0.89	-
WS-T3-S2		test14	15.2	152	152	0.50	0.278	No	0.256	2 of 4[3]	2.58	0	0.88	-
WS-T4-S1	4	test12	15.2	152	152	0.50	0.278	No	0.256	2 of 4[2]	2.58	0	-	0.87
WS-T4-S2		test13	15.2	152	152	0.50	0.278	No	0.256	2 of 4[2]	2.58	0	-	0.89
WP-T5-N0-S1	5	test9	15.2	137	122	0.44	0.278	No	0.227	-	2.58	0	0.97	-
WP-T5-N0-S2		test10	15.2	137	122	0.44	0.278	No	0.227	-	2.58	0	-	-
WP-T5-N5-S1		test7	15.2	137	122	0.44	0.278	No	0.227	-	2.58	5	1.51	-
WP-T5-N5-S2		test8	15.2	137	122	0.44	0.278	No	0.227	-	2.58	5	1.59	-
WP-T5-N10-S1		test5	15.2	137	122	0.44	0.278	No	0.227	-	2.58	10	1.83	-
WP-T5-N10-S2		test6	15.2	137	122	0.44	0.278	No	0.227	-	2.58	10	1.93	-
												Average	1.31	0.88
												Std. Dev	0.38	0.02

[1] Shear span-to-depth ratio
[2] Weakened plane joint at wall-pedestal interface
[3] Weakened plane joint at wall midheight
[4] Nominal shear strength per FEMA356
[5] Nominal shear friction capacity per ACI318-05

Measurements from local instrumentation revealed that the lateral displacement of the spandrels of Types 1, 2, 3, as well as the piers (Type 5), was governed by shear deformations associated with diagonal cracking, followed by widening of and sliding along the diagonal cracks. For these specimen types, the contribution of flexural deformations and sliding along the WPJ were found to have minor influence on the overall wall displacement history, particularly in the nonlinear response range. For all of these specimens, lateral load failure (degradation of lateral load capacity) was associated with crushing of concrete close to the center of the wall, followed by spalling of diamond-shaped wedges of concrete (Fig. 2(a)) on both sides. The lateral load behavior and failure mode of Type-4 spandrel specimens (WPJ located at the wall-pedestal interface) was unique. The lateral stiffness of these specimens was reduced significantly when a large visible crack formed (at 0.2% drift) across the entire length of the WPJ (Fig. 2(b)). Applying larger drift levels resulted in sliding along the WPJ, with no other form of relevant damage observed at any other location. Measurements from local sensors confirmed that the lateral displacement of these walls was governed by sliding along the WPJ.

Figure 2.   Typical failure mode. (a) Type 1 wall at 2.0% lateral drift (typical for types 1, 2, 3, 5), (b) Type 4 wall at 3.0% lateral drift.

Shear Strength of the Test Specimens

Comparisons of the maximum lateral load measured for each test (average of positive and negative loading directions) with the nominal (per FEMA 356) shear strength of the specimens ($V_{TEST}/V_{n,FEMA}$) are presented in Table 1. The measured-to-nominal (per ACI 318) shear-friction capacity comparisons ($V_{TEST}/V_{n,ACI-SF}$) for Type-4 specimens, which experienced shear-friction failure along the weakened plane joint located at the wall-pedestal interface, are also included in the table. It must be noted that part of the longitudinal web reinforcement (4 out of 6 bars for Types 1 and 2, and 2 out of 4 bars for Types 3 and 4) were not continuous over the entire height of the spandrels; that is, they were cut at the weakened plane joint to provide a crack initiation plane. This can be interpreted as a reduction in the effective area of the longitudinal web reinforcement, which reduces the longitudinal reinforcement ratio of Type-1 spandrels to 0.14%, Type-2 spandrels to 0.13%, and Type-3 and Type-4 spandrels to 0.13%. Based on common interpretations of the ACI 318-08 code, the shear strength should be based on the minimum value of the web reinforcement ratios (provided that the yield strength of the transverse and longitudinal reinforcement is the same), and considering that FEMA 356 recommends using a minimum reinforcement ratio of 0.15% for the shear strength calculation, the expected shear strength of the spandrel specimens ($V_{n,FEMA}$) was calculated using a reinforcement ratio of 0.15%. A reinforcement ratio of 0.15% was also used for the FEMA shear strength calculation of the pier specimens, since no hooks were provided on the transverse web reinforcement of the piers (as well as spandrels of Types 3 and 4), and thus, the reinforcement might not be capable of reaching the yield stress at potential diagonal crack locations.

Nominal shear strength – Overall average of the results presented in Table 1 indicate that the FEMA nominal shear strength calculation ($V_{n,FEMA}$) provides a lower-bound estimate of the measured lateral load capacity of the spandrel and pier specimens that failed in shear.

Effect of lack of hooks on web reinforcement on shear strength – Spandrel specimens of Types 2 and 3 have longitudinal web reinforcement ratios of 0.4% and 0.26%, respectively, when the effective reduction in the amount of longitudinal reinforcement due to discontinuity of longitudinal bars at the weakened plane joint is ignored. Unlike Type-2 spandrels, 180-degree hooks are not provided on the transverse web reinforcement of Type-3 spandrels. However, average $V_{TEST}/V_{n,FEMA}$ values obtained for Type-2 and Type-3 spandrels are 1.00 and 0.88, respectively. Considering that the boundary reinforcement ratio of Type-2 specimens (1.70%) is slightly larger than that of Type-3 specimens (1.33%), it appears that the lack of 180-degree looks on the transverse web reinforcement of Type-3 spandrels does not have a significant influence on their measured shear strength.

Effect of discontinuity of web reinforcement on shear strength – Hooks were also not provided on the transverse web reinforcement of the pier (Type 5) specimens, and longitudinal web reinforcement ($\rho_l = 0.23\%$) was continuous over the specimen height, since a weakened plane joint was not provided. Comparing results of the Type-5 pier specimen with zero axial load ($V_{TEST}/V_{n,FEMA} = 0.97$) with average results of Type-3 spandrels ($V_{TEST}/V_{n,FEMA} = 0.89$) with the weakened plane joints ($\rho_l = 0.26\%$ with 2 out of 4 longitudinal web bars discontinued), it is apparent that discontinuity of the longitudinal web bars at the weakened plane joint has some negative influence on the expected shear strength of the walls, although the results could have also been influenced by amount of boundary reinforcement ratio.

Nominal shear-friction capacity – For the Type-4 spandrel specimens that failed in shear-friction across the weakened plane joint at the wall-pedestal interface, the ACI nominal shear-friction capacity calculation ($V_{n,ACI-SF}$) slightly overestimates the lateral load capacities measured during testing. Weakened plane joints were also provided along the mid-height (when oriented vertically) of spandrel specimens of Types 1, 2, and 3. Types 3 and 4 were identical except for the location of the weakened plane joint. Type-3 specimens failed in shear (with diagonal cracks propagating across the WPJ with no significant deviation in crack path and direction, and crushing of concrete at wall mid-height at ultimate), and exhibited lateral load capacities larger than their calculated ACI nominal shear-friction capacities. Type-4 specimens, on the other hand, failed to reach their calculated shear friction capacities. The initiation of flexural yielding immediately triggered a sliding shear mechanism prior to crushing of concrete in the compression zone.

Lateral Deformation Attributes of the Test Specimens

Lateral Load vs. Displacement Envelope

FEMA 356 (section 2.8.3) recommends characterization of the lateral load-displacement envelope (or backbone curve) for specimens tested under reversed cyclic loading, via intersecting the first load-displacement cycle at drift level "i" with the second load-displacement cycle at drift level "i-1". This approach results in a curve that falls inside the full cyclic response, which in some cases, may result in backbone curves that not follow the general trend. This inconsistency for the current test results is depicted in Fig. 3(a) (backbone/FEMA). Based on this shortcoming, a different approach was proposed to characterize the backbone curve for the current tests. In this approach, the maximum displacement (displacement reversal) points are first selected for all first and second cycles at all drift levels. The maximum displacement point for the first cycle is assigned as a point on the backbone curve. Accounting for degradation is included by using the average of the lateral load values measured from the first and second cycles, only if the average falls below the 80% of the maximum lateral load. If there is one cycle prior to failure, it is assumed that the second cycle is under zero lateral load.
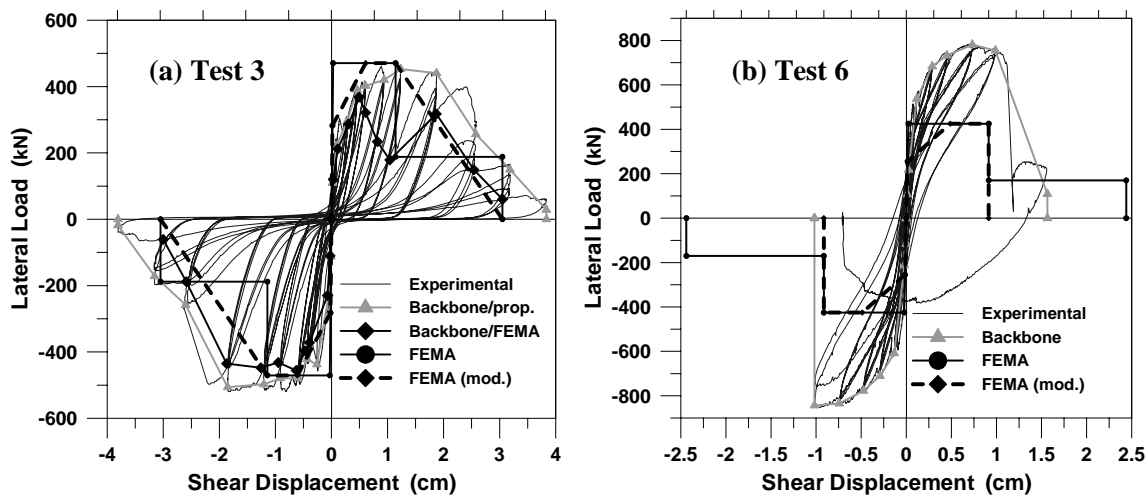

Figure 3.   Measured response and derived backbone curves for shear: (a) Test 3, (b) Test 6.

Accordingly, Fig. 3 also shows the load-displacement response of selected specimens

(test 3 and test 6) based on the procedure described. As can be seen in the figure, relatively smooth backbone curves, which are more representative of the cyclic test results, was obtained following the procedure proposed (Fig. 3(a), Backbone/prop.), as opposed to the inconsistencies observed in the FEMA procedure (Fig. 3(a), Backbone/FEMA).

Shear and Flexural Deformation Components

Fig. 4 shows the shear and flexural deformation contributions of the lateral load vs. top displacement response measured for Test 6. The cracked flexural stiffness value $(0.5E_cI_g)$ suggested by FEMA 356 (Table 6-5) is also plotted in the figure for comparison. The flexural deformation contribution to top displacement is mostly linear, although the flexural stiffness is noticeably reduced after cracking. The test results show a softer stiffness, even for cycles prior to first observation of diagonal cracking. This was found to be due to rotation at the wall-pedestal interfaces resulting from strain penetration of the wall longitudinal reinforcement embedded in the pedestal. The shear stiffness $(0.4E_cA_w)$ suggested by FEMA (FEMA 356, Table 6-5) is also plotted in Fig. 4(a) for comparison. As it can be seen, all specimens show good agreement between the experimental results and the elastic shear stiffness, confirming that that the elastic stiffness term can be used for the initial loading cycles.
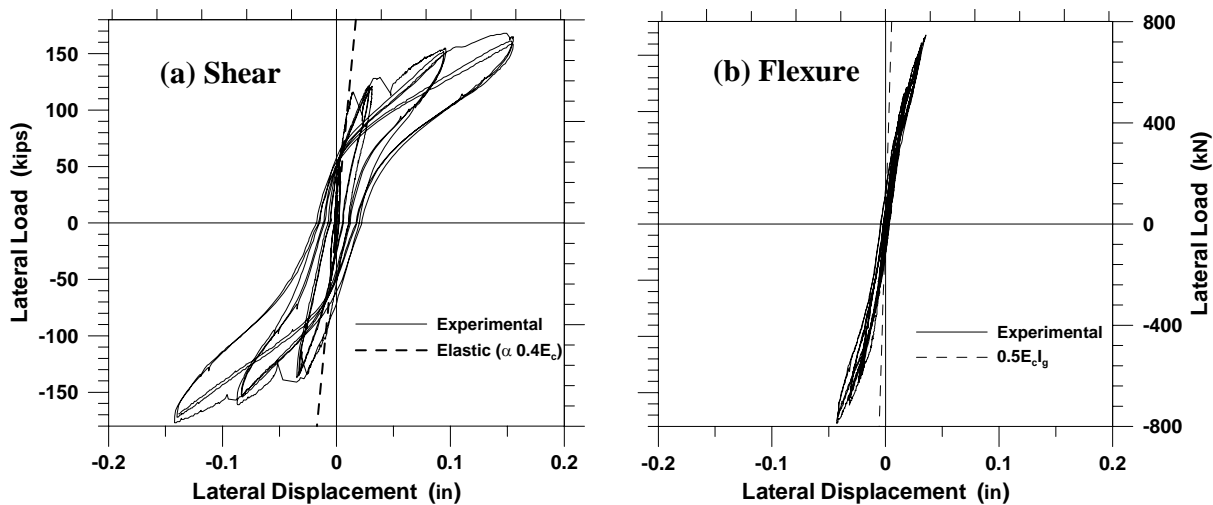

Figure 4.   Lateral deformation components for test 6: (a) shear, and (b) flexure.

Shear Backbone Curve

The overall lateral load versus top displacement results are used to determine their shear deformation component, over the entire range of drift levels, by subtracting a representative response of the flexural deformation component of top displacement, which is formulated as a linear model, after a best fit of the experimental data. The FEMA 356 model for shear-dominated walls, and modified as suggested here to account for cracking, is compared to the experimental response. In general, the peak capacity is reached at approximately 0.4% drift in all cases, and degradation is usually observed at about 0.75%.

Specimens that have experienced a higher level of flexural cracking (e.g., in test 3 and

more significantly in test 14) or shear sliding (e.g., test 12) possess delayed degradation characteristics. After degradation, although the drop in the lateral load is abrupt, the load is generally regained, although to levels slightly lower than that for previous cycles for specimens without axial load (e.g., test 1, test 3 and test 14). Thus, for such specimens, a portion of the lateral load carrying capacity is maintained during subsequent cycles. Subsequent cycles yield a lateral load, degradation which is somewhat less sudden than what is suggested by FEMA 356 (see Fig. 3). The progression of degradation suggests rather a linear variation from the maximum lateral load capacity to almost zero lateral load at the maximum drift cycle, than a sudden drop in the lateral load to a residual level. The specimens with axial load (test 6 and test 8), on the other hand, were not able to reach the maximum drift level (2% drift) suggested by FEMA. In those cases, an abrupt drop in lateral load is observed after about 0.75% drift, followed by a rapid degradation of the lateral load after relatively few cycles, which results in a negative stiffness at the end of the test. Once the negative stiffness is observed, the lateral load degrades rapidly to zero, and axial collapse occurs due to the failure of the specimen to maintain the constant axial load applied. This observation leads to the idea of limiting the drift capacity to 0.75% drift in specimens with considerable axial load, that is, axial load higher or equal than 5% of the axial load capacity ($5\%A_gf'_c$). For specimens without considerable axial load (less than $5\%A_gf'_c$), it is reasonable to estimate a linear degradation from the maximum capacity to zero lateral load, once a 2% drift has been reached. These considerations are incorporated as modifications to the original backbone curve proposed by FEMA (see Fig. 3). The modifications also incorporate the change in stiffness due to cracking as discussed earlier; that is, the cracking point is set at 60% of the lateral load capacity, and a linear variation is assumed until the capacity is reached at 0.4% drift. The modified FEMA curve is plotted in the figures together with the original formulation for comparison, revealing reasonable and representative backbone estimates. It is important to notice that the shear strength is not captured accurately by FEMA 356 for test 6 (Fig. 3(b)), since the influence of axial load is not considered in the FEMA shear strength prediction.

Analytical Modeling of the Test Specimens

An analytical model that couples wall flexural and shear responses was proposed by Massone *et al*. (2006) based on framework proposed by Petrangeli *et al*. (1999) The model incorporates RC panel behavior into a two-dimensional macroscopic fiber model (i.e., Multiple Vertical Line Element Model or MVLEM, Orakcal *et al*., 2004), in order to capture the experimentally observed shear-flexure interaction in RC walls. The model formulation involves modifying the MVLEM by assigning a shear spring to each macro-fiber of the MVLEM element (Fig. 5). Each macro-fiber is then treated as a RC panel element, subjected to membrane actions; that is, in-plane uniform normal and shear stresses (Fig. 5). Therefore, the interaction between flexure and shear is incorporated at the fiber level. To represent constitutive panel behavior, a rotating-angle modeling approach (i.e., Modified Compression Field Theory, Vecchio and Collins 1986) can be used. For each constitutive RC panel element, a uniaxial constitutive stress-strain model for concrete is applied along the principal directions to obtain the stress field associated with the principal directions, assuming that the principal stress and strain directions coincide. For reinforcing steel, a uniaxial constitutive stress-strain model is applied in the directions of the reinforcing bars, based on the assumption of perfect bond between reinforcing steel and concrete. The presence of the weakened plane joint (WPJ) and the unfavorable anchorage condition due to discontinuity of the longitudinal web reinforcement at the WPJ on

the spandrel specimens, were not considered in the analysis.

As described by Massone *et al*. (2006), the deformations or strains within the components of each panel element are determined from the six prescribed degrees of freedom, (u_x, u_y and θ at both ends of the model element) as shown in Fig. 5. Assuming that the shear strain is uniform along the section and that plane sections remain plane, the longitudinal normal (axial) strain (ε_y) and shear distortion (γ_{xy}) components of the strain field are calculated for the entire section (for all the strips (i)) based on the prescribed degrees of freedom for the current analysis step. The transverse normal strain within each strip (ε_x) is initially estimated to complete the definition of the strain field, allowing stresses and forces to be determined from the constitutive material relationships and geometric properties (dimensions and reinforcement and concrete areas for each strip). A numerical solution procedure (e.g., Newton-Raphson method) can be employed to linearize the equilibrium equation and iterate on the unknown quantity ε_x (transverse normal strain in each strip i), to achieve horizontal equilibrium for a given resultant transverse normal stress, σ_x (resultant of transverse normal stress components in concrete and reinforcing steel), within each strip. In the case where the transverse normal strains are known, this iteration is not required.
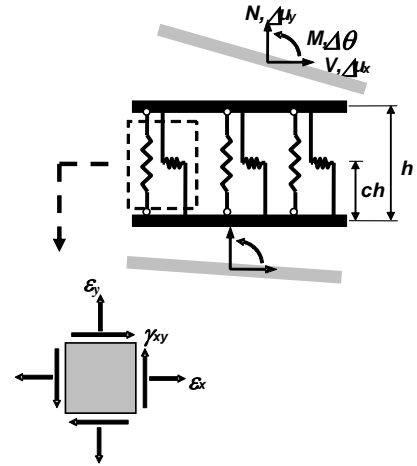

Figure 5. Coupled model element

Model Results with Zero Transverse Normal Stress or Strain

The experimental results demonstrated that the end pedestal at the top and bottom of the walls restrained the transverse normal strains. The model formulation described previously, which assumes zero transverse normal stress resultant ($\sigma_x = 0$), does not account for this effect, producing a softer and weaker analytical load versus displacement response than measured (average strength ratio, V_{MODEL}/V_{TEST}, of 0.71, with a ratio under 1.0 for all specimens). A stiffer and stronger response is expected for the condition where the constraint of the end blocks ($\varepsilon_x = 0$) is considered (V_{MODEL}/V_{TEST} of 1.34, with a ratio over 1.0 for all specimens).

Model Results with Measured Transverse Normal Strains and Interface Rotational Springs

The experimental lateral load vs. top displacement responses tend to be softer than the model predictions that incorporate measured average transverse normal strains (ε_x^{exp}), especially for the flexural deformations (Fig. 6). A review of the experimental results reveals that the contribution of flexural deformations to the top displacement is concentrated within the first pair of gauges located at the boundaries of the test specimens. Given that these sensors span the wall-pedestal interface, the potential contribution of the extension of the longitudinal reinforcing bars within the pedestals to lateral displacements measured over the wall height, was investigated. Experimentally and analytically calibrated expressions of transverse normal strain can be found elsewhere (Massone *et al*., 2009; Massone, 2010). The extension of the longitudinal reinforcing bars within the pedestals was modeled to consider strain penetration only, given that enough

embedment length was provided to prevent bond slip failure. The strain penetration model, which is rather simple, did not consider bond slip or bond stress variation along the bars embedded within the pedestal, as traditional bond slip models do. Instead, a linear strain variation for the embedded longitudinal bars was used to account for pedestal flexibility within the vicinity of the reinforcement. Such an approach was incorporated to capture the experimentally observed behavior and to account for the imperfection in the test setup, since the pedestals were not actually rigid enough to promote a fixed boundary condition; however, this approach may not be necessary for system modeling studies, where the flexibility of all components are considered. To model the impact of rebar extension (strain penetration) within the pedestals, a moment-curvature analysis was conducted at the wall-pedestal interfaces. A cracked section was considered together with a linear strain distribution along the embedment length of the longitudinal bars within the top and bottom pedestals, in order to define a linear rotational spring.
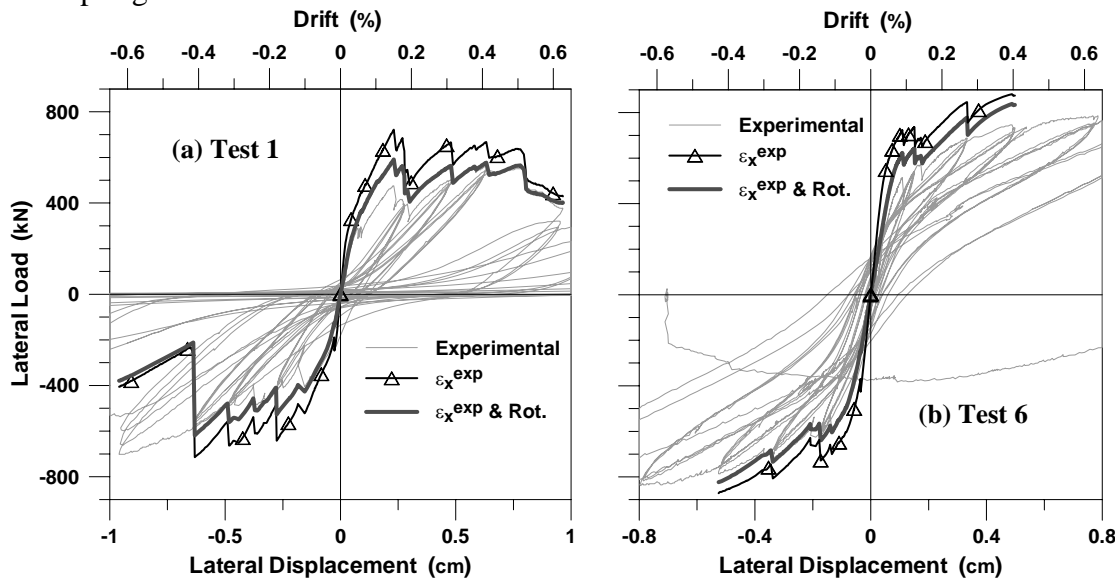

Figure 6.   Load vs. top displacement (selected displacement range): (a) Test 1, and (b) Test 6.

As seen in Fig. 6, implementation of the interface springs (denoted in the figure as ε_x^{exp} & *Rot.*) improves the agreement between the model response prediction and the experimental results for both lateral stiffness and lateral load capacity. Regarding the lateral load capacity, peak strength predicted using the model with the interface rotational springs is about 5% to 10% lower than the model without the interface rotational springs, and better represents the experimental results. The lateral strength ratio (V_{MODEL}/ V_{TEST}) of specimens ranges from 0.97 to 1.23 with an average of 1.07 with low dispersion. The flexural and shear components were also studied, and results reveal that the rotational spring substantially improves the flexural component of wall, which total flexural component may account for up to 50% of lateral deformations at low drift levels. At larger drift level the response is controlled by shear that accounts for the majority of the top displacement (80 to 90%).

Conclusions

An experimental program was conducted and supplemented with analytical modeling

studies in order to assess the lateral load responses of lightly reinforced wall pier and spandrels with outdated construction details. The findings of this program are summarized as follows:

1) Discontinuity of a portion of the longitudinal web reinforcement at a possible weakened plane joint and the lack of hooks on transverse reinforcement may have some negative influence on the expected shear strength of wall segments expected to fail in diagonal tension; but the influence is rather modest (in the range of 10% for the specimens tested). Particular attention must be paid to the evaluation of the shear strength of wall segments with weakened plane joints (with part of the longitudinal web reinforcement discontinued), particularly at locations where moment demands are critical. Under these conditions, the wall segments are prone to an early sliding shear type of failure following flexural yielding.

2) The backbone curve proposed by FEMA might not be conservative for wall with axial load. The proposed expression limits the ductility of axially loaded walls, and also better captures the degradation of walls without axial load. In order to correctly capture the flexural initial stiffness (which might account for up to 50% of the initial displacement) the extension (strain penetration) of the rebar embedded in the pedestals must be accounted for, resulting in an initial flexural stiffness prediction close to half of a cracked section.

3) For the shear-flexure interaction model proposed, the overall load-displacement responses obtained from the model were improved, resulting in a lateral strength ratio (V_{MODEL}/V_{TEST}) average of 1.07 by using the experimentally measured average transverse normal strain and incorporating a rotational spring at the wall-pedestal interfaces to account for strain penetration within the pedestals. Good stiffness predictions were also observed in the flexural and shear components.

References

Vecchio, F. J., and Collins, M. P., 1986. The modified compression-field theory for reinforced concrete elements subjected to shear, *Journal of the American Concrete Institute* 83 (2), 219-231.

Petrangeli, M., Pinto, P. E., and Ciampi, V., 1999. Fiber element for cyclic bending and shear of RC structures I: theory, *ASCE Journal of Engineering Mechanics* 125 (9), 994-1001.

Massone, L. M., 2006. RC wall shear–flexure interaction: analytical and experimental responses, *Ph.D. Thesis*, University of California, Los Angeles.

Orakcal, K., Wallace, J. W., 2006. Flexural modeling of reinforced concrete walls – experimental calibration, *ACI Structural Journal* 103 (2) 196-206.

Massone, L. M., Orakcal, K., and Wallace, J. W., 2006. Shear-flexure interaction for structural walls, *ACI Special Publication – Deformation Capacity and Shear Strength of Reinforced Concrete Members Under Cyclic Loading* SP-236, 127-150.

Orakcal, K., Massone, L. M., and Wallace, J. W., 2009. Shear strength of lightly reinforced wall piers and spandrels, *ACI Structural Journal* 106 (4), 455-465.

Massone, L. M., Orakcal, K., and Wallace, J. W., 2009. Modeling of squat structural walls controlled by shear, *ACI Structural Journal* 106 (5), 646-655.

Massone, L. M., 2010. Strength prediction of squat structural walls via calibration of a shear-flexure interaction model, *Engineering Structures* (in press).